



Effect of slide burnishing method on the surface integrity of AISI 316Ti chromium–nickel steel

J. T. Maximov¹ · G. V. Duncheva¹ · A. P. Anchev¹ · N. Ganev² · I. M. Amudjev¹ · V. P. Dunchev¹

Received: 4 December 2017 / Accepted: 15 March 2018 / Published online: 21 March 2018
© The Brazilian Society of Mechanical Sciences and Engineering 2018

Abstract

Chromium–nickel steels are widely used in various fields of the engineering practice because of their increased corrosion resistance. One of the most used chromium–nickel steel is AISI 316Ti. It is known from the engineering practice that processing this steel by cutting creates difficulties and problems. However, there is no information regarding the effectiveness of the slide burnishing (SB) method in terms of quality of the processed surface of this chromium–nickel steel. A comprehensive experimental and FEM study of the surface integrity of slide burnished specimens made of AISI 316Ti austenitic stainless steel has been carried out. The effect of the SB parameters on the obtained roughness, microhardness, residual stress, fatigue strength (life) and wear resistance has been studied. A fully coupled thermal-stress FEM analysis has been conducted to be appreciated the effect of the generated temperature in SB process on the residual stress formation. The SB of AISI 316Ti steel achieves: roughness of $R_a = 0.055 \mu\text{m}$; micro-hardness increased by more than 32%; significant wear resistance; introduced residual stress with a maximum absolute value, which significantly exceeds the yield limit of the bulk material; increased fatigue strength by 38.9%; fatigue life increasing more than 385 times. The obtained experimental outcomes for the main characteristics of the surface integrity prove that SB can be successfully applied as a mixed burnishing for finishing symmetrical rotational components made of chromium–nickel steels.

Keywords AISI 316Ti steel · Slide burnishing · Surface integrity · High-cycle fatigue performance · Wear resistance · Fully coupled thermal-stress FEM analysis

List of symbols

a_p	Cutting depth (mm)	m_i	Mass after friction path (mg)
A	Area (m^2)	n	Number of passes
A_5	Elongation (%)	N_i	Number of cycles to failure
c	Specific heat ($\text{J/kg}^\circ\text{C}$)	P	Normal load (N)
E	Young's modulus (Pa)	q_g	Heat flux density (W/m^2)
f	Feed rate (mm/rev)	r	Tool radius (mm)
F_b	Burnishing force (N)	R_a	Surface roughness (μm)
I_r	Specific wear resistance (Nm/mg)	R_a^{init}	Initial surface roughness (μm)
k	Thermal conductivity ($\text{W/m}^\circ\text{C}$)	s_i	X-ray elastic constants (TPa^{-1})
L	Friction path (m)	v	Burnishing velocity (m/min)
m	Mass wear (mg)	z	Transverse contraction (%)
m_0	Mass before friction (mg)	α_t	Coefficient of thermal expansion ($\text{m/m}^\circ\text{C}$)
		Δs	Slip increment (m)
		Δt	Time increment (s)
		ε_{nom}	Nominal strain
		ε_{ln}	Logarithmic strain
		$\varepsilon_{\text{ln}}^p$	Logarithmic plastic strain
		η	Coefficient
		θ	Temperature ($^\circ\text{C}$)
		ν	Poisson's ratio
		ρ	Density (kg/m^3)

Technical Editor: Márcio Bacci da Silva.

✉ J. T. Maximov
maximov@tugab.bg; jordanmaximov@gmail.com

¹ Technical University of Gabrovo, 5300 Gabrovo, Bulgaria

² Czech Technical University in Prague, Prague, Czech Republic

τ	Friction stress (Pa)
φ_i	Coefficients
σ_e	Fatigue limit (Pa)
σ_{true}	True stress (Pa)
σ_u	Ultimate stress (Pa)
σ_Y	Yield limit (Pa)
ω	Angular velocity (s^{-1})

1 Introduction

Chromium–nickel steels are widely used in various fields of the engineering practice—food, chemical, automotive, nuclear and traditional energy industries, household appliances, instrumentation, etc., because of their increased corrosion resistance. The requirements to the surface layers of components made of these steels, the most common are low roughness, high micro-hardness, wear resistance, and fatigue strength.

These requirements are satisfied largely by burnishing technologies based on surface plastic deformation (SPD). The latter is mechanical surface treatment in which a hard deforming element presses over a workpiece surface to induce plastic deformation in the surface layer. That results in improved finish, enhanced hardness and compressive residual stresses. SPD is carried out through two groups of methods: dynamical (for instance, shot peening, laser peening, water cavitation peening) and static (roller burnishing, ball burnishing, slide burnishing). The main advantage of the dynamical methods is that they can be applied for processing of complex surfaces without limitation. For improving surface integrity of symmetrical rotational components the static methods are more suitable. According to Ecoroll's classification [1], two processes exist: roller burnishing and deep rolling. The main objective of roller burnishing is to produce “burnishing”, wherein the roughness is reduced considerably. The other attributes of the surface layer (increased micro-hardness, compressive residual stresses) inherent in the SPD also exist, but are rather concomitant and not significant. Deep rolling aims primarily increasing the fatigue strength, since this process produces three effects simultaneously: burnishing, cold work, compressive residual stresses with maximum magnitude in absolute value and of considerable depth. According to Korzynski [2, 3], the burnishing methods can be classified as smoothing, dimensional, hardening, and mixed. Although in the engineering practice slide burnishing (SB) is usually perceived as “smoothing burnishing” [3], the various combinations of SB governing parameters can implement different processes [4, 5]. Therefore, SB can be implemented for both smoothing burnishing and mixed burnishing, depending on the

governing factors combination. For instance, SB increases the fatigue strength of 2024-T3 cyclic bending specimens with 44%—from 180 to 260 MPa and at the same time, fatigue life is increased more than 200 times compared to specimens processed only by cutting [5]. The essential difference between deep rolling and SB is determined by the type of contact between the workpiece and the deforming element, i.e., rolling contact and sliding friction contact, respectively. SB is kinematically similar to turning, but instead of a cutting tool blade, spherical ended tip of a deforming element is moved under pressure over the worked surface causing plastic deformation on the surface and subsurface layers (Fig. 1).

Slide burnishing devices and tools are compatible with every conventional and CNC-controlled lathes or CNC turning center. Therefore, a workpiece can be slide burnished in one setting directly after machining. SB is especially suited for shafts and large bores, and can be implemented to flat face surfaces. SB is a very economical method for producing mirror-like surface finishes on a wide range of ferrous and nonferrous machined surfaces. Since set up and operation is relatively simple, and cycle times are short, no special operator skills are required. The governing factors of the SB process are basic and additional: sphere radius of the deforming element r , mm; burnishing force F_b , N; feed rate f , mm/rev; burnishing velocity v , m/min. The number of passes, working scheme and lubricant are the additional factors.

Relative to chromium–nickel steels, SPD is most often accomplished through ball and roller burnishing. Saï and Lebrun [6] studied the effect of ball burnishing on surface

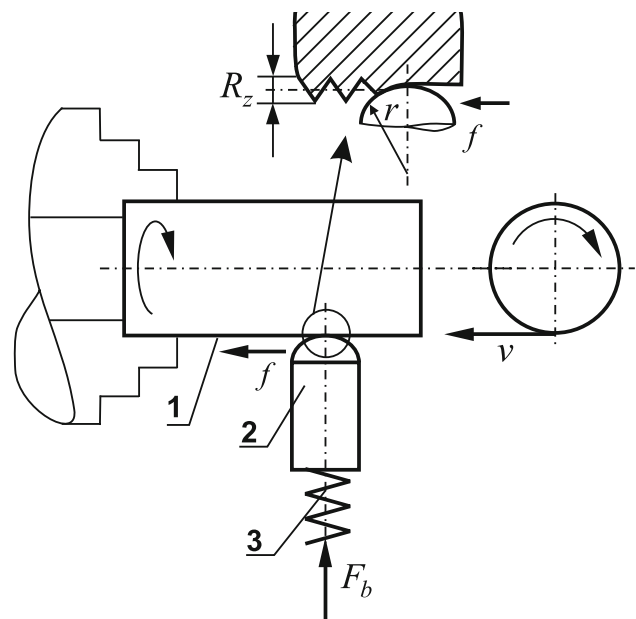


Fig. 1 Scheme of the SB

characteristics of duplex stainless steel. From an initial roughness of $R_a = 0.68 \mu\text{m}$ after turning, respectively, $0.59 \mu\text{m}$ after grinding, they have achieved roughness up to $R_a = 0.17 \mu\text{m}$, respectively, $0.16 \mu\text{m}$, using ball burnishing. An HV 0.2 hardness testing has shown increasing the micro-hardness from about 580 (after grinding) to about 700 after ball burnishing. The latter (after turning), has introduced compressive hoop and axial residual stresses in a depth of $600 \mu\text{m}$. It should be noted that, in fact, the authors have carried out the deep rolling process, according to Ecoroll's classification. Shiou and Hsu [7] developed sequential ball grinding, ball burnishing and spherical polishing ultra-precision method for improving the surface roughness of STAVAX stainless steel. The authors have improved the surface roughness R_a of the ball burnished specimen from about 0.12 to $0.022 \mu\text{m}$ using the optimal spherical polishing parameters. Tian and Shin [8] applied roller burnishing and laser-assisted burnishing to MP35N nickel-base alloy and AISI 4140 steel to improve the surface finish. The authors have proved that it is very difficult to achieve a surface finish of less than $0.3 \mu\text{m}$ on the MP35N specimen by conventional roller burnishing, while laser-assisted burnishing has achieved a roughness R_a of up to $0.18 \mu\text{m}$. The authors have conducted a hardness test with a load of 1 kgf. At initial hardness of 450 HV, they have obtained the maximum hardness of about 520 on the MP35N specimen by roller burnishing and about 540 by laser-assisted burnishing. For a hardened AISI 4140 steel, at initial hardness of 410, they have achieved hardness of about 460 HV. After roller burnishing, the authors have measured in the surface layer residual compressive stresses as follows: hoop—about 200 MPa; axial—about 600 MPa. Shiou et al. [9] have developed a new ball burnishing tool to improve the surface integrity of the fine turned AISI 420 stainless steel. They reported that the surface roughness can be improved from $R_a = 1.1$ to $R_a = 0.025 \mu\text{m}$ and the surface hardness can be increased from 51 to 52.5 HRC. The authors have measured residual stresses (probably axial) of up to -1047 MPa. It is noteworthy that SB is used relatively more rarely. Labanowski and Ossowska [10] studied the effect of slide diamond burnishing on stress corrosion cracking susceptibility of duplex stainless steel.

One of the most used chromium–nickel steel is AISI 316Ti. It is known from the engineering practice that the processing this steel by cutting creates difficulties and problems. However, there is not information regarding the technological potentialities of the SB method in terms of quality of the processed surface of AISI 316Ti austenitic stainless steel. That is why the main objective of this study is to establish the effect of the SB process parameters on the surface roughness, micro-hardness, residual stresses, fatigue performance and wear resistance, obtained in slide

burnishing of AISI 316Ti austenitic stainless steel and thus, an evaluation of the effectiveness of slide burnishing as “mixed burnishing” to be made.

2 Experiment

2.1 Material

The material under consideration is AISI 316Ti austenitic stainless steel (EN/DIN X6CrNiMoTi 17-12-2, Mat. No/W. Nr 1.4571), supplied as cold drawn bar. Chemical composition and mechanical characteristics were established at our laboratory “Testing of Metals”. The chemical composition is (in percent): C 0.026; Si 0.56; Mn 1.9; P 0.101; S 0.145; Cr 16.671; Mo 2.19; Ni 10.55; Co 0.202; Cu 0.33; Ti 0.112; V 0.081; W 0.093 and Rest < 67.039. Tensile tests (at room temperature) on specimens with diameter $d = 6$ mm and base $\ell = 6d$ recorded the following average mechanical characteristics: Young's modulus $E = 1.86 \times 10^5$ MPa; yield limit $\sigma_Y = 510$ MPa; ultimate stress $\sigma_u = 642$ MPa; elongation $A_5 = 38\%$; transversely contraction $z = 73.4\%$.

2.2 Roughness

2.2.1 Machine tool and slide burnishing device

The experiment was conducted on CNC T200 lathe using a special SB device [4]. The device (Fig. 2) is mounted on the tool post of the lathe. A polycrystalline diamond tool with spherical tip is supported elastically in the device. The required burnishing force was set by deforming an axial spring with linear behavior, situated in the device. The diamond burnishing point is brought into contact with the specimen at its centerline and normal to the surface being treated. The device is then fed into the specimen an

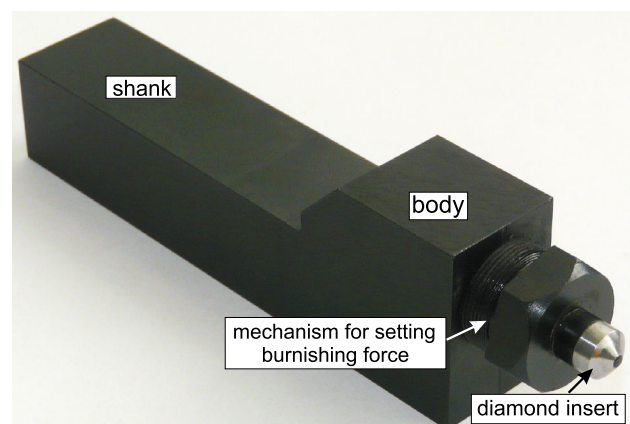


Fig. 2 SB device

additional 0.05 mm to allow the diamond tool to become disengaged from the stop in the device. The latter is then fed along the surface of the rotating specimen to produce a burnished surface.

Machining trials were carried out on the specimens made of AISI 316Ti steel. The specimens have a length of 200 mm and diameter of 40 mm. Each specimen was clamped to one side with the chuck and supported on the other side. Turning as pre-machining and slide burnishing were carried out in one clamping process to minimize the concentric run-out in burnishing. The turning was conducted from end to end of each specimen, while the treated length through slide burnishing with one combination of governing factors was 20 mm. Thus, for a group of experimental points (combinations of governing factors) one and the same initial roughness before burnishing was ensured.

CCMT120408-F2 carbide cutting insert was used for turning. Pre-machining was conducted with a constant feed rate $f = 0.1$ mm/rev, cutting speed $v_c = 90$ m/min and cutting depth $a_p = 0.25$ mm. The cutting edge radius was $r_c = 0.8$ mm.

The surface roughness on R_a criterion in axial direction was measured using Mitutoyo Surftest—4. Each experimental value of R_a was obtained in the following way: the measurement was taken on three generatrices at 120° as for each generatrix the mean value of the roughness was given; the final value of the roughness was obtained as an arithmetic mean of the obtained roughness for the three generatrices.

2.2.2 Methodology of the roughness study

An extended experiment to determine the roughness obtained by SB was carried out. In the previous studies of SB process [4, 10], it is established that the basic factors in order of importance under “roughness obtained” criterion are arranged as follows: radius r , burnishing force F_b , feed rate f , burnishing velocity v . Based on this information, the following method of study of the roughness is developed in the present work: the SB optimal basic parameters under “minimum roughness” criterion are defined by means a one-factor-at-the-time methodology consistently for all factors, in order of their significance. Thus, starting from the most significant factor, the study proceeds following “the funnel principle”: at the entrance, the irrational combinations are quickly eliminated and the optimal combination of factor levels is localized around the funnel top. This iterative approach combines a detailed scanning of the factor space with a relatively rapid elimination of irrational combinations of factors. Thus, after the first iteration, the factor space is significantly reduced. The proposed approach was conducted in three steps:

- In the first step a one-factor-at-the-time methodology was applied to screen the influence of the two most important factors: radius and burnishing force. These factors were changed of 5 levels in the selected intervals of variation (Table 1), while the feed rate and burnishing velocity remained constant values—about the optimal for high-strength aluminium alloys [4] and 37Cr4 steel [10];
- In the second step the effect of the feed rate on the roughness obtained was established. The best five combinations from radius and burnishing force in step 1, ensuring minimum roughness, are selected. With each from these 5 combinations the feed rate was changed of 5 levels in the interval $f \in [0.02, 0.1]$. Thus, the first three factors (r , F_b and f) form a total of new 25 combinations;
- In the third step the influence of burnishing velocity on the roughness obtained was found. The best five combinations of radius, burnishing force and feed rate in step 2, ensuring minimum roughness, are selected. With each from these 5 combinations the burnishing velocity was changed of 5 levels in the interval $v \in [50, 250]$. Thus, the four basic factors (r , F_b , f and v) form a total of new 25 combinations. The combination, which ensures minimal roughness, gives optimal values of the basic factors.

Finally, using optimal basic SB parameters the effect of the additional parameters on the roughness obtained was established.

2.3 Micro-hardness

After slide burnishing, micro-hardness was measured on the processed cylindrical surface applying HV 0.05 hardness testing. RMT-3 micro-hardness tester was used. A quantitative criterion for increasing micro-hardness is the surface micro-hardness increase coefficient k_h

$$k_h = \frac{HV - HV_{init}}{HV_{init}} 100 \%, \quad (1)$$

where HV_{init} is the initial micro-hardness (after cutting); HV is the micro-hardness after SB.

Table 1 Machining parameters for slide burnishing

Process parameter	Levels				
Sphere radius of the diamond r (mm)	1	2	3	4	5
Burnishing force F_b (N)	50	100	150	200	250

2.4 Residual stresses

The residual hoop and axial stresses in the surface and subsurface layers of the burnished specimens were measured using the X-ray diffraction technique. To analyze the stress gradients beneath the samples surface, the layers of material were gradually removed by electrolytic polishing.

Using MnK α radiation, X'Pert PRO MPD diffractometer was used to measure lattice deformations in austenite. The average penetration depth of X-ray radiation was approximately 5/11 μm (Fig. 3). Diffraction angles $2\theta hkl$ were determined from the peaks of the diffraction lines $K\alpha 1$ of planes {311}. Diffraction lines $K\alpha 1$ were fitted by Pearson VII function and Rachinger's method was used for separation of the diffraction lines $K\alpha 1$ and $K\alpha 2$. For residual stress determination, Winholtz and Cohen method and X-ray elastic constants $1/2s_2 = 6.98 \text{ TPa}^{-1}$, $s_1 = -1.87 \text{ TPa}^{-1}$ were used. The samples were analyzed in the axial and tangential directions.

Parameters of the device settings were as follows: θ – θ diffractometer X'Pert PRO MPD in Bragg–Brentano focusing geometry; pinhole $2 \times 1 \text{ mm}^2$, non-diffracted silicon mask of diameter 6.5 mm; without a monochromator; β -filter (absorbing diffracted $K\beta$ radiation) located in front of the proportional detector.

Parameters of the experiment were as follows: range $2\theta = 147^\circ/157^\circ$; tilts $\sin^2 \psi = 0, 0.2, 0.4, 0.6$ of both positive and negative values of angle ψ .

2.5 Fatigue behavior

For bending fatigue testing hour-glass shaped specimens with minimum diameter of 7.5 mm were prepared (Fig. 4).

Fatigue tests were carried out under rotating beam loading ($R = -1$) at a frequency of about 100 Hz in air. For producing S – N curves, one specimen was tested at each stress amplitude. In the case where there was an apparent difference between the anticipated and the actual results (large scattering), the test with the same amplitude was repeated.

2.6 Wear resistance

A comparative study of the mass wear and wear resistance of samples made of AISI 316Ti austenitic stainless steel was carried out under dry friction conditions. The samples were cut out from slide burnished work pieces as it is shown in Fig. 5. The specimen sizes are $10 \times 10 \times 22 \text{ mm}$. One of the specimens (basic one) was produced only by cutting, and the other four samples were slide burnished using the optimal SB parameters with different working schemes and different number of passes. The specimens were denoted as follow: (A) basic specimen; (B) slide burnished with one pass; (C) one-way working scheme and $n = 6$; (D) two-way working scheme and $n = 4$; (E) two-way working scheme and $n = 6$. The study was carried out on “thumb-disk” tribotester according to the functional scheme shown in Fig. 6. The specimen is fixed to the holder which is placed in the loading head. The specimen front surface contacts with the working surface of the abrasive body which is fixed to a horizontal disk. The latter rotates at a constant angular velocity around its vertical center axis. The normal load P is applied in the center of the contact area of the specimen, and the friction path is set by the number of cycles of the cyclometer.

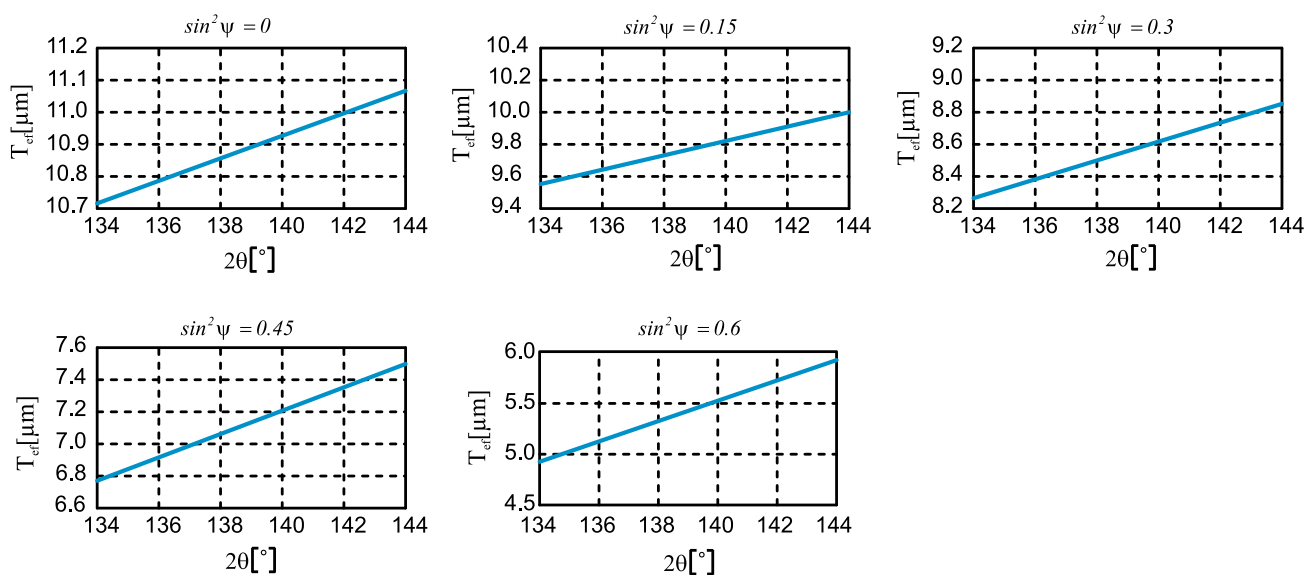


Fig. 3 Average penetration depth of X-ray radiation

Fig. 4 Fatigue specimen sizes

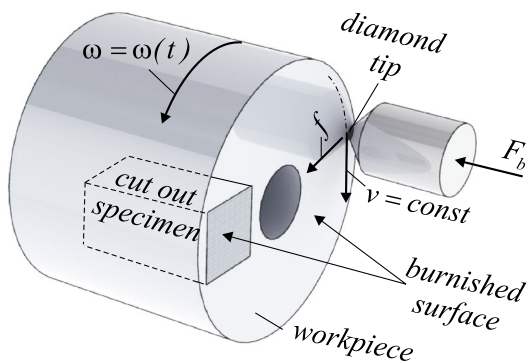
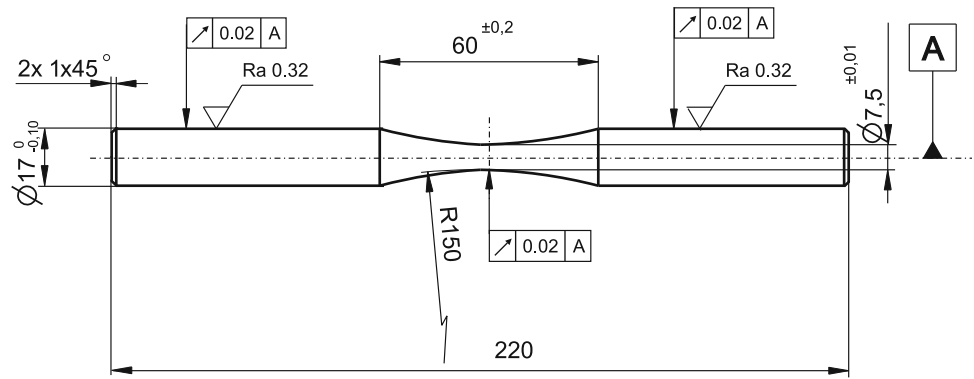


Fig. 5 Specimen for wear resistance testing

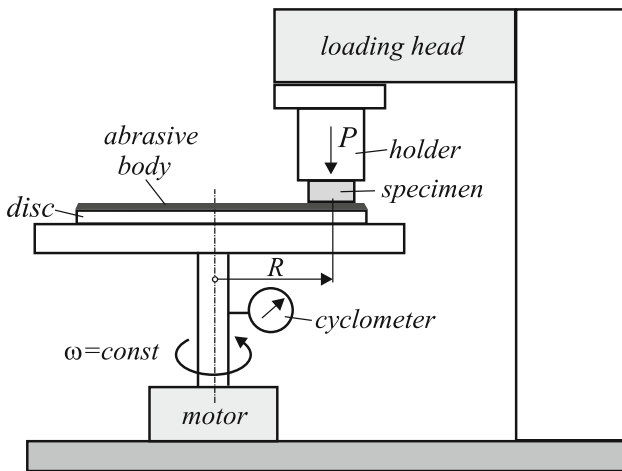


Fig. 6 Functional scheme of “thumb-disk” tribo-tester

The experiment was carried out under the following conditions (conformable to specific application): nominal contact area $A = 1 \times 10^{-4} \text{ m}^2$, sliding velocity $v = 0.155 \text{ m/s}$; friction path $L = 10.68 \text{ m}$, $L = 21.35 \text{ m}$, $L = 42.70 \text{ m}$; normal load $P = 4.57 \text{ N}$; abrasive surface type—Corundum P 320. The electronic balance with accuracy of 0.1 mg was used for measurement the mass of the specimens before friction, m_0 , and after the corresponding number of cycles (friction path), m_i . Before each

measurement, the samples were cleaned from mechanical and organic particles and dried with ethyl alcohol to be prevented the electrostatic effect.

3 Results and discussion

In this section, the obtained experimental outcomes for roughness, micro-hardness, residual hoop and axial stresses, fatigue strength/life and wear resistance are shown and analyzed.

3.1 Roughness

3.1.1 SB optimal parameters

3.1.1.1 First step The effect of burnishing force and diamond radius was established in this step. Their levels are shown in Table 1. Feed rate and burnishing velocity retain constant values, respectively, $f = 0.05 \text{ mm/rev}$ and $v = 100 \text{ m/min}$. Number of passes is $n = 1$. A lubricant-cooler Hacut 795-H was used in all three steps. The average initial roughness was $R_a^{\text{init}} = 0.528 \mu\text{m}$. The roughness obtained outcomes are depicted in Fig. 7. As a whole, the combinations comprising radius $r = 1 \text{ mm}$ with all values of burnishing force lead to greatly deteriorated roughness. At the same time all combinations comprising radius $r = 4 \text{ mm}$, significantly reduce initial (after turning) roughness. The five combinations, ensuring lowest roughness, are depicted in Table 2.

3.1.1.2 Second step The effect of feed rate on the roughness obtained is studied in this step. The feed rate levels are shown in Table 3. Each of the five combinations from r and F_b , depicted in Table 2, is combined with the feed rates from Table 3. The burnishing velocity remains constant— $v = 100 \text{ m/min}$. Table 4 shows the input SB factors, used in this second iteration. Number of passes is $n = 1$. The initial roughness R_a^{init} was between 0.54 and 0.68 μm . The roughness obtained is shown in Fig. 8a. The

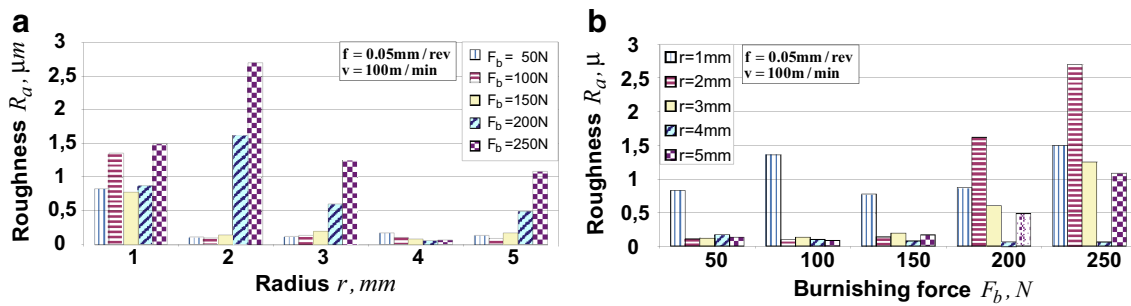


Fig. 7 Roughness obtained depending on: a tool radius; b burnishing force

Table 2 The best five combinations of r and F_b

Combinations			Roughness R_a (μm)
No	r (mm)	F_b (N)	
1	4	200	0.057
2	4	250	0.062
3	4	150	0.077
4	5	100	0.084
5	2	100	0.094

$f = 0.05$ mm/rev; $v = 100$ m/min

Table 3 Levels of the feed rate

Process parameter	Levels				
	1	2	3	4	5
Feed rate f (mm/rev)	0.02	0.04	0.06	0.08	0.1

combinations, containing $r = 2$ mm and $F_b = 100$ N, are not depicted in Fig. 8a, since they give obviously worse results for the roughness. The five combinations of r , F_b and f , ensuring minimum roughness, are shown in Table 5.

3.1.1.3 Third step The influence of burnishing velocity on the roughness obtained is investigated in this step. The burnishing velocity levels are depicted in Table 6. Each of

the five combinations from r , F_b and f from Table 5 is combined with the velocities from Table 6. Number of passes is $n = 1$. Table 7 shows the input SB factors, used in this third step. The initial roughness R_a^{init} was between 0.55 and 0.66 μm . The roughness obtained is shown in Fig. 8b. Apparently, the combination $r = 4$ mm, $F_b = 200$ N and $f = 0.06$ mm/rev provides the lowest roughness. For the whole range of variation of burnishing velocity, the obtained roughness varies in a narrow interval: $R_a \in [0.057, 0.074]$ μm . The roughness decreases with increasing the velocity, as for $v = 200$ m/min the roughness is minimum: $R_a = 0.057$ μm . For the maximum velocity from the range of variation, the roughness slightly increases. Larger burnishing velocity leads to larger strain velocity and more generated heat, which negatively affect the micro-hardness, residual stresses and fatigue strength of the processed surface. On the other hand the productivity of processing is larger.

3.1.2 Effect of SB additional parameters

With the selected optimal basic parameters ($r = 4$ mm; $F_b = 200$ N; $f = 0.06$ mm/rev) and with burnishing velocity from the middle of the interval ($v = 150$ m/min), the influence of the number of passes n and working scheme (one-way and two-way [4]) on the roughness obtained was studied. A lubricant-cooler Hacut 795-H was used. The outcomes are depicted in Fig. 9. Obviously, one-

Table 4 Input SB factors used in the second step

No	1	2	3	4	5	6	7	8	9	10	11	12	13
r (mm)	4	4	4	4	4	4	4	4	4	4	4	4	4
F_b (N)	200	200	200	200	200	250	250	250	250	250	150	150	150
f (mm/rev)	0.02	0.04	0.06	0.08	1	0.02	0.04	0.06	0.08	1	0.02	0.04	0.06
No	14	15	16	17	18	19	20	21	22	23	24	25	
r (mm)	4	4	5	5	5	5	5	2	2	2	2	2	
F_b (N)	150	150	100	100	100	100	100	100	100	100	100	100	
f (mm/rev)	0.08	1	0.02	0.04	0.06	0.08	1	0.02	0.04	0.06	0.08	1	

$v = 100$ m/min

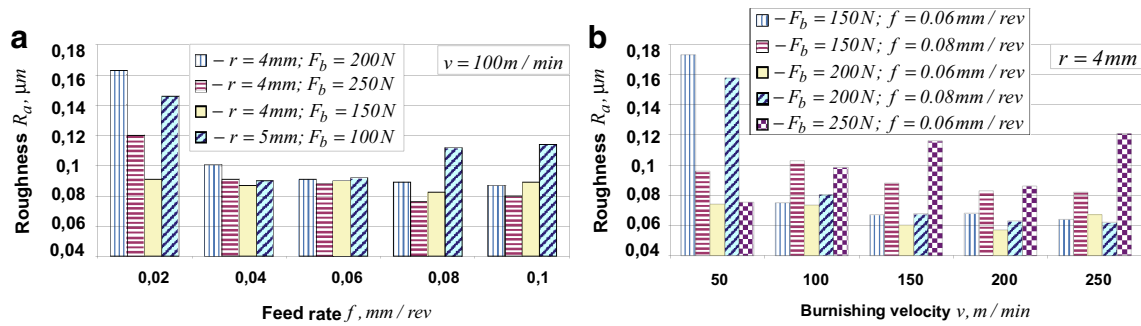


Fig. 8 Roughness obtained depending on: a feed rate; b burnishing velocity

Table 5 The best five combinations of r , F_b and f

Combinations				Roughness R_a (μm)
No	r (mm)	F_b (N)	f (mm/rev)	
1	4	150	0.06	0.085
2	4	150	0.08	0.081
3	4	200	0.06	0.091
4	4	200	0.08	0.089
5	4	250	0.06	0.088

$v = 100$ m/min

Table 6 Levels of the burnishing velocity

Process parameter	Levels				
	1	2	3	4	5
Burnishing velocity v (m/min)	50	100	150	200	250

way scheme provides a lower roughness, whereby the number of passes has no practical significance for the roughness. Conversely, two-way scheme leads to a higher roughness. With increasing the number of passes, the roughness increases slightly.

Table 7 Input SB factors used in the third step

No	1	2	3	4	5	6	7	8	9	10	11	12	13
F_b (N)	150	150	150	150	150	150	150	150	150	150	200	200	200
f (mm/rev)	0.06	0.06	0.06	0.06	0.06	0.08	0.08	0.08	0.08	0.08	0.06	0.06	0.06
v (m/min)	50	100	150	200	250	50	100	150	200	250	50	100	150
No	14	15	16	17	18	19	20	21	22	23	24	25	
F_b (N)	200	200	200	200	200	200	200	250	250	250	250	250	
f (mm/rev)	0.06	0.06	0.08	0.08	0.08	0.08	0.08	0.06	0.06	0.06	0.06	0.06	
v (m/min)	200	250	50	100	150	200	250	50	100	150	200	250	

$r = 4$ mm

3.2 Microhardness

Using the optimal SB parameters ($r = 4$ mm; $F_b = 200$ N; $f = 0.06$ mm/rev), four specimens are slide burnished with different burnishing velocities. The samples have a diameter of 30 mm and a length of 40 mm. For each specimen the surface micro-hardness is measured in 20 points and the arithmetic mean is calculated. The influence of the burnishing velocity on the surface micro-hardness is depicted in Fig. 10a. Obviously, with increasing the velocity, the micro-hardness decreases. At velocity $v = 200$ m/min the measured micro-hardness (387 HV 0.05) is less than that of the base specimen, processed only by cutting (412 HV 0.05). Therefore, when the goal is to achieve the maximum micro-hardness of the slide burnished layer, it is advisable to work with a smaller burnishing velocity, for instance $v = 50$ m/min. The resulting roughness at that velocity is $R_a = 0.072$ μm , and the surface micro-hardness increase coefficient is $k_h = 14.6\%$.

Figure 10b shows the influence of number of passes and the working scheme on the surface micro-hardness. Five samples were used, one of which was processed only by cutting. The other four were slide burnished using one-way and two-way working schemes, each of which with number of passes $n = 2$ and $n = 6$. SB process was fulfilled with the selected optimal basic parameters, whereupon the burnishing velocity was $v = 100$ m/min. Obviously, with increasing the number of passes the micro-hardness

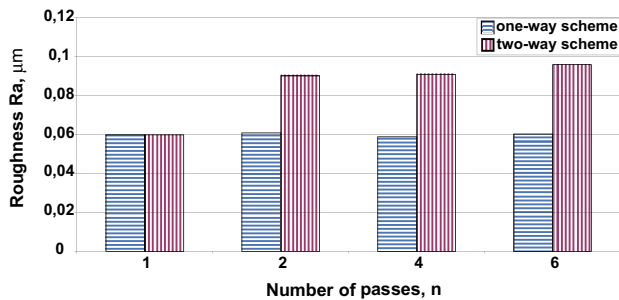


Fig. 9 Roughness obtained depending on number of passes ($r = 4$ mm; $F_b = 200$ N; $f = 0.06$ mm/rev; $v = 150$ m/min)

increases due to strain hardening of the material being slide burnished. The maximum magnitude of the surface microhardness increase coefficient is obtained for $n = 6$ (one-way scheme): $k_h = 32.52\%$, whereby the resulting roughness is $R_a = 0.06$ μm (see Fig. 9).

3.3 Residual stresses

The specimens were slide burnished with the selected optimal burnishing parameters ($r = 4$ mm; $F_b = 200$ N; $f = 0.06$ mm/rev), but with different burnishing velocities. Residual stress distribution is depicted in Fig. 11. The axial stresses are significantly larger in absolute value compared to the hoop normal stresses at the points from the surface layer. The two types of stresses practically are equalized after 220 μm depth. The compressive zone has a depth greater than 620 μm . For both types of stresses the larger burnishing velocity causes reduction of the residual stresses in the surface and subsurface layers to a depth of about 60 μm . The big burnishing velocity causes two effects: larger strain velocity in the surface layer and more generated heat. The first effect is expressed in an increase of the yield limit of the deformed micro-volume of material, and the result is a lesser degree of plastic deformation. The

second effect is expressed in creation of tensile thermal stresses in the surface layer. As a result, both effects lead to a reduction of the beneficial compressive residual stresses in the surface layer.

3.4 Fatigue behavior

Four groups of specimens were manufactured. The first group was treated only by cutting on a CNC T200 lathe. By means of CCMT120408-F2 carbide cutting insert, having a round cutting edge, an average roughness of $R_a = 0.8$ μm was achieved. This group, called “basic”, serves as a reference condition (RC) to which the other three groups of specimens were compared. The specimens from the second group were slide burnished with the optimal values of the basic governing process parameters ($r = 4$ mm; $F_b = 200$ N; $f = 0.06$ mm/rev; $v = 100$ m/min). Number of passes was $n = 1$. A polycrystalline diamond was used as a deforming element in the SB process. A lubricant Hacut 795-H was used. The third and the fourth groups were burnished as the second group, but with number of passes $n = 2$ and $n = 4$, respectively. SB was conducted using two-way working scheme [4].

The Wöhler’s (S–N) curves are shown in Fig. 12 comparing the four groups of specimens. The reference condition has a 10^7 cycles fatigue strength (this is fatigue limit σ_e for a steel) of 270 MPa. After SB with number of passes $n = 1$, the fatigue limit increases with 29.6%—from 270 to 350 MPa. At the same time, the fatigue life is increased by more than 166 times. The increase is due to the reduced surface roughness, the introduced beneficial residual stresses and the increased surface layer micro-hardness due to strain hardening. After SB with number of passes $n = 2$, significant increase in the fatigue limit was obtained compared to RC—from 270 to 370 MPa: the fatigue limit increases with 37% and the fatigue life—by more than 333 times. After SB with number of passes $n = 4$, the fatigue limit increases with 38.9%—from 270 to 375 MPa. The

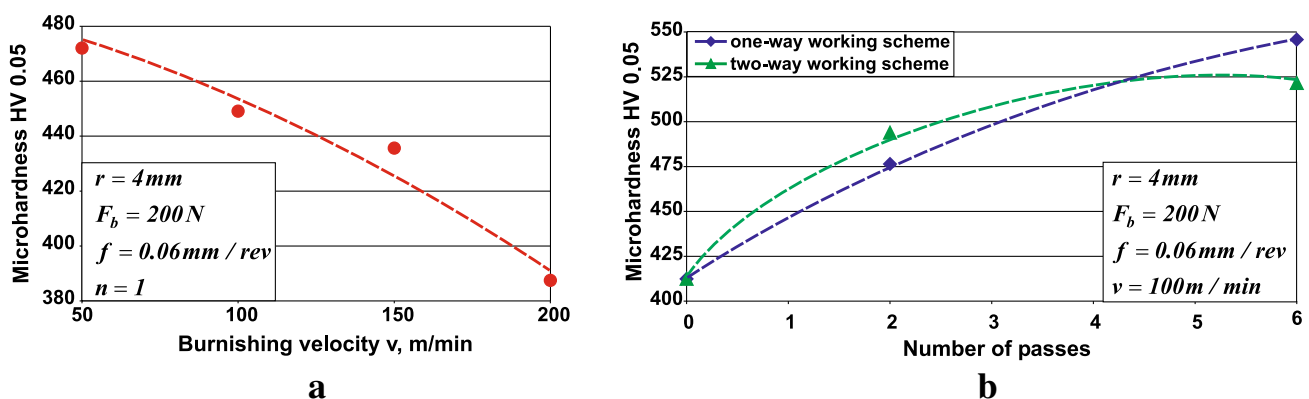
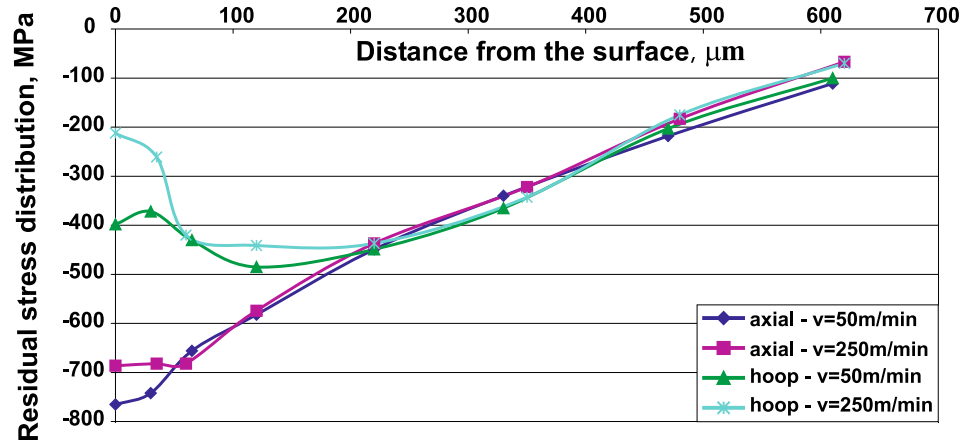


Fig. 10 Micro-hardness obtained depending on: **a** burnishing velocity; **b** number of passes and working scheme

Fig. 11 Residual stress distribution obtained by X-ray diffraction stress analysis



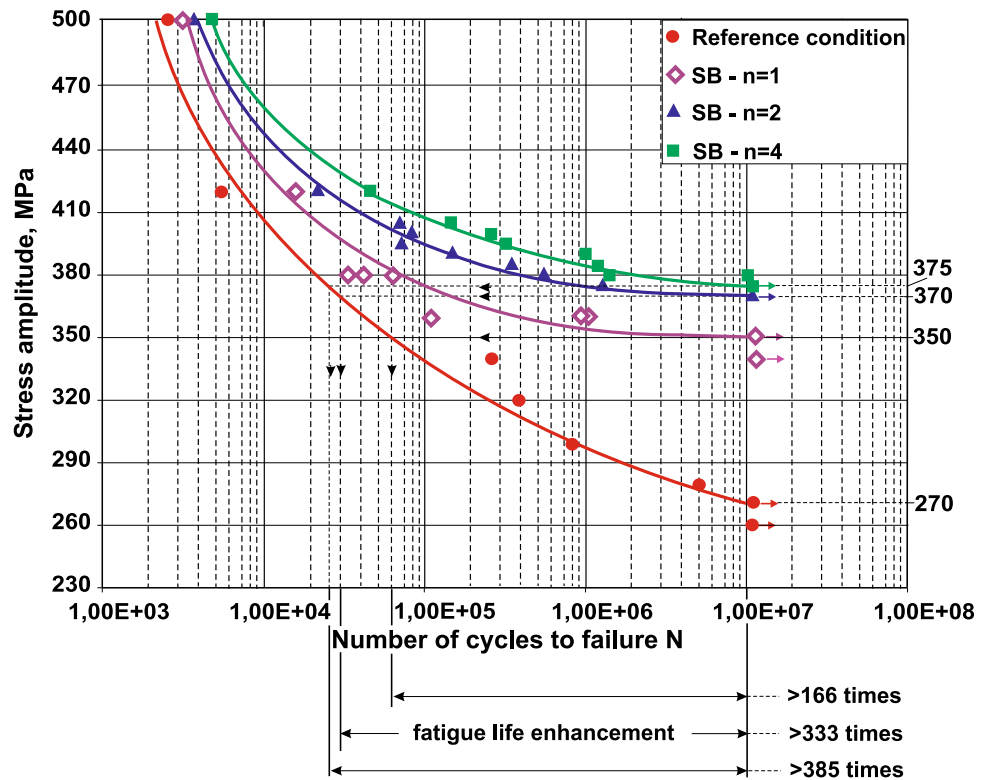
fatigue life is increased by more than 385 times. Obviously, a further increase in number of passes is not advisable.

3.5 Wear resistance

The following characteristics are defined: mass wear $m = m_0 - m_i$, mg; specific wear resistance $I_r = \frac{PL}{m}$, Nm/mg. The experimental outcomes for the mass wear depending on the friction path and for specific wear resistance are shown in Fig. 13. The mass wear m of all specimens subjected to SB is less pronounced than that of the basic specimen (A) for friction path $0 < L \leq 21.35$ m (Fig. 13a). The exception is specimen (C) for $26 < L$

≤ 42.7 m, which is slide burnished by means of one-way working scheme and number of passes $n = 6$. As a whole, a steady tendency with smallest amount of wear for the whole friction path is observed for the specimen (B) which is slide burnished with one pass. The mass wear of specimen (B) compared to specimen (A) is 1.31/1.64 times less for the whole friction path. This reflects in a high specific wear resistance I_r of specimen (B) (Fig. 13b). The experimental results for the mass wear m and the specific resistance are similar for the specimens burnished with two-way scheme: specimen (D)— $n = 4$ and specimen (E)— $n = 6$. Therefore, from the point of view of wear resistance of AISI 316 Ti steel, it is appropriate to carry out the SB

Fig. 12 S–N curves



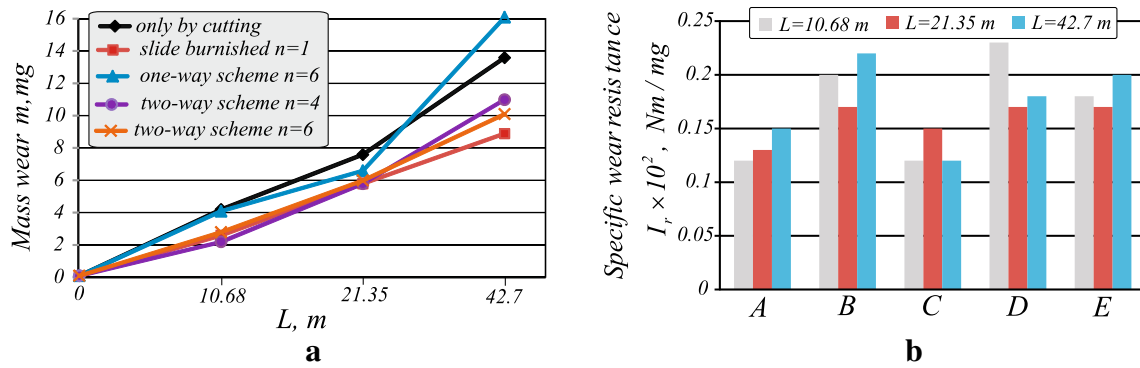


Fig. 13 Experimental outcomes for: **a** mass wear and **b** specific wear resistance, obtained by the following input SB parameters: $r = 4 \text{ mm}$; $F_b = 200 \text{ N}$; $f = 0.06 \text{ mm/rev}$

process either with one pass or by means of two-way working scheme and number of passes $n = 6$.

4 Finite element method analysis of the influence of burnishing velocity on the residual stresses

The purpose of this section is to be appreciated the effect of the generated temperature in SB process on residual stress formation. In other words, the aim is to estimate the effect of the burnishing velocity on the residual stress distribution.

The nature of the SB is different in comparison with this of roller burnishing or deep rolling. The tangential contact between the deforming element and the surface being treated is sliding friction. Regardless of the low coefficient of friction in a case of using synthetic diamond [10] the work of the friction forces is significant and dissipates into a heat. Therefore, the deforming process in SB has a thermo-mechanical nature. The heat generated is the reason for the emergence of thermoplastic deformations, which influence the formation of the residual stress field. Therefore, a fully coupled thermal-stress FEM analysis has been used to determine the thermo-mechanical effect in SB process.

This procedure is used to simultaneously find displacements/stresses on one hand, and the temperature field when these two categories strongly influence each other on the other. The heat transfer between the contacting surfaces of the diamond and the workpiece is defined as:

$$q_g = k(\theta_A - \theta_B), \tag{2}$$

where q_g is the heat flux density generated by the friction, passing from point A from one surface at a point B from the other surface; θ_A and θ_B are temperatures of the two points; k is the conductivity of the gap between the two surfaces.

The generated by the friction heat flux is:

$$q_g = \eta \tau \dot{s} = \eta \tau \frac{\Delta s}{\Delta t}, \tag{3}$$

where $0 < \eta \leq 1$ is a coefficient, showing what proportion of the work of friction dissipates into a heat, τ is stress from friction, Δs and Δt are, respectively, increments of the slip and the time.

For both contacting surfaces:

$$q_{g,i} = \phi_i q_g, \quad i = 1, 2. \tag{4}$$

In the conducted FEM simulations, it is assumed that $\phi_1 = \phi_2 = 0.5$ and $\eta = 1$.

3D FE model is depicted in Fig. 14. From the specimen, starting from the surface layer, a prismatic body with sizes of $5 \times 3 \times 3 \text{ mm}$ is cut off. Since the specimen diameter is considerably larger than the diamond spherical tip, the body surface coinciding with the specimen surface is assumed to be flat. The diamond radius and burnishing force are, respectively, $r = 3 \text{ mm}$ and $F_b = 200 \text{ N}$. The burnishing force is set by means of the diamond depth of penetration. Their interdependence is established through a preliminary FE analysis (static general). A single relative movement between a deforming element and the body in the direction of its large size is considered. Because of the symmetry, only the half of the “deforming element-work piece” system is modeled. The FE model consists of 5420 linear hexahedral coupled temperature-displacement elements of type C3D8T and 7623 nodes. A purely elastic behavior is assumed for the deforming diamond element. Young’s modulus is $E = 10.5 \times 10^{11} \text{ Pa}$ and is assumed to be temperature-independent. Poisson’s ratio is $\nu = 0.1$. The density and the coefficient of thermal expansion are, respectively, $\rho = 3515 \text{ kg/m}^3$ and $\alpha_t = 1 \times 10^{-6} \text{ m/(m}^\circ\text{C)}$. The specific heat c and the conductivity k with isotropic behavior are temperature-dependent (Table 8).

The behavior of the prismatic body is assumed to be temperature-dependent and rate-independent. Young’s modulus E , coefficient of thermal expansion α_t ,

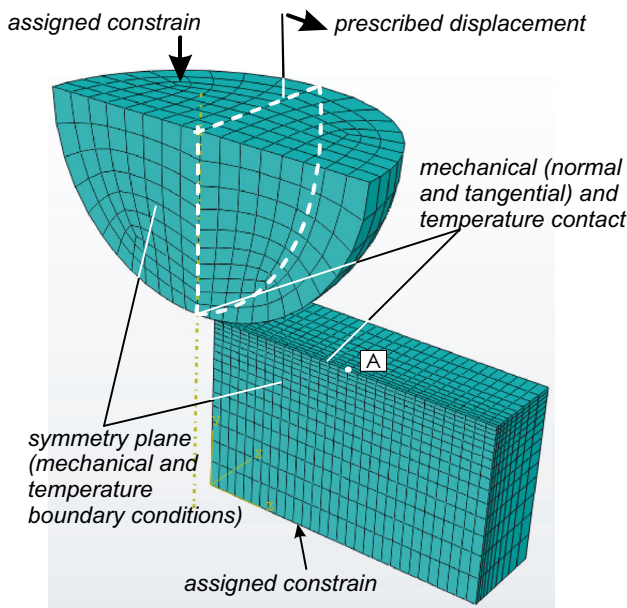


Fig. 14 3D FE model

conductivity k and specific heat c are shown in Table 9. Poisson’s ratio is $\nu = 0.3$.

Because of the characteristics of ABAQUS v.6.12.1, the fully coupled thermal-stress FEM analysis can not be conducted with a nonlinear kinematic/isotropic with cyclic hardening behavior. Therefore, in this analysis isotropic strain hardening was used. Since the objective was a comparison of the residual stress fields for two cases of heat generation (with and without friction), the error introduced by the adoption of isotropic hardening does not matter. For the same reason (a comparison of the residual stress fields for two cases) the material constitutive model is defined for the bulk material by means of temperature-dependent tensile tests instead of the instrumented indentation test and inverse FEM analysis. The role of the initial roughness (after turning) in the FE model is very important for the resulting characteristics (after burnishing) in the surface layer. However, the used 3D FE model pursues another objective, mentioned above.

The nominal stress-nominal strain temperature-dependent curves for AISI 316Ti austenitic stainless steel are obtained at Metal Testing Laboratory at the Technical University of Gabrovo (Fig. 15). The stress measure in

Table 8 Temperature-dependent specific heat and conductivity for the diamond element

T (°C)	0	50	200	400	600
c (J/kg °C)	420	600	1000	1500	1650
k (W/m ² °C)	2500	2000	1400	1000	600

ABAQUS v. 6.5-1 is Cauchy or “true” stress, which corresponds to the force per current area, and the strain measure is a logarithmic strain. If nominal stress-nominal strain ($\sigma_{nom} - \epsilon_{nom}$) data are available, a simple conversion to true stress-logarithmic strain ($\sigma_{true} - \epsilon_{ln}$) data exists:

$$\sigma_{true} = \sigma_{nom}(1 + \epsilon_{nom}), \tag{5}$$

$$\epsilon_{ln} = \ln(1 + \epsilon_{nom}). \tag{6}$$

Logarithmic plastic strain values are used in ABAQUS to define the strain hardening behavior:

$$\epsilon_{ln}^p = \epsilon_{ln} - \frac{\sigma_{true}}{E}, \tag{7}$$

where E is Young’s modulus. A nonlinear isotropic hardening model of elastic–plastic rate-independent material is defined. These data are entered in ABAQUS as a temperature-dependent point set ($\sigma_{true} - \epsilon_{ln}$).

Two types of contacts are defined between the deforming element and the prismatic body: mechanical—a normal and a tangential one with friction coefficient of $\mu = 0.052$ assigned in accordance with [11]; thermal-heat generation from friction with coefficients $\eta = 1$ and $\phi_1 = \phi_2 = 0.5$, and heat transfer between the surfaces of the deforming element and the specimen with the heat transfer coefficients, changing in a linear law from the clearance between them:

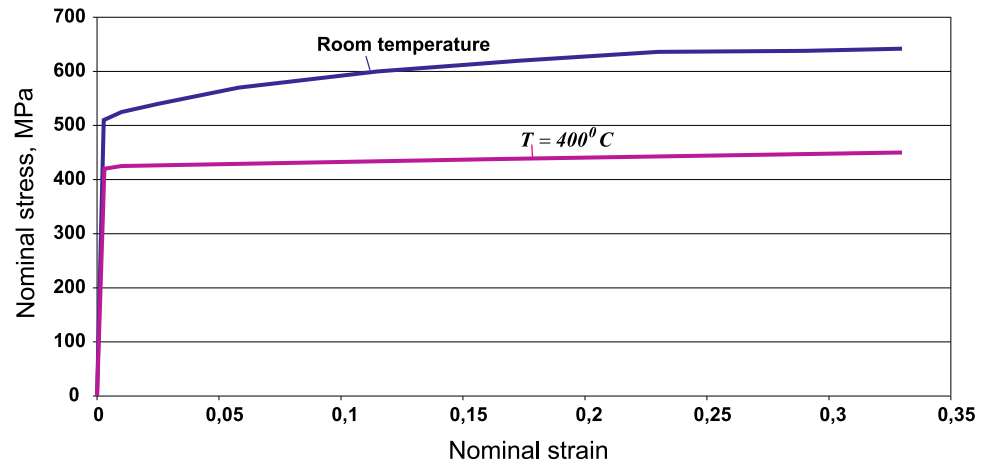
$$\text{conductivity} = \begin{cases} 50 \text{ W}/(m \text{ } ^\circ\text{C}) \Rightarrow \text{clearance} = 0 \\ 0 \text{ W}/(m \text{ } ^\circ\text{C}) \Rightarrow \text{clearance} = 0.0001 \text{ m} \end{cases}$$

The burnishing velocity ($v = 300$ m/min) is defined through an assigned displacement of the plane symmetry of the deforming element and the real time for passing in direction of the large size of the specimen. Due to the very little time for the process (for the treated length of 5 mm and sliding velocity of 300 m/min the time is 0.001 s) the convection and radiation are ignored. The initial temperature is 0 °C.

The change in the temperature at a point A from the specimen surface is shown in Fig. 16. The maximum temperature increase is 120 °C. The residual hoop stress distribution is depicted in Fig. 17. Curve 1 shows residual hoop stress distribution when the friction coefficient is $\mu = 0.052$ and the basic process parameters are: radius $r = 3$ mm, burnishing force $F_b = 200$ N and burnishing velocity $v = 300$ m/min. Curve 2 shows residual hoop stress distribution for the same basic process parameters, but when the tangential contact is frictionless, i.e., in the absence of heat generation. Apparently the generated heat leads to a significant reduction of the residual stresses at the points of the surface layer. This effect was confirmed by the experiment (see Fig. 11). Therefore, the increase of the burnishing velocity leads to smaller in absolute value

Table 9 Temperature-dependent properties for the prismatic body

T ($^{\circ}\text{C}$)	0	20	100	200	300	400
E (GPa)	186	186	185.5	177.5	166	153
α_t [$\text{m}/(\text{m } ^{\circ}\text{C})$]	16×10^{-6}	16×10^{-6}	16.5×10^{-6}	17.5×10^{-6}	18×10^{-6}	18.5×10^{-6}
k [$\text{W}/(\text{m } ^{\circ}\text{C})$]	15	15	–	–	–	21.5
c [$\text{J}/(\text{kg } ^{\circ}\text{C})$]	480	–	–	–	–	660

Fig. 15 Nominal stress-nominal strain temperature-dependent curves

residual stresses in the surface and subsurface layers to a depth of approximately 0.2 mm. After this depth the generated heat obviously has no practical significance.

5 Conclusions

A comprehensive experimental and FEM study of the surface integrity of slide burnished specimens made of AISI 316Ti austenitic stainless steel has been carried out. On the basis of the obtained results the following conclusions can be made:

- The optimal magnitudes of the SB process basic parameters have been found on minimum roughness criterion. Of the four SB basic parameters, the

burnishing speed is the most insignificant factor. By means of the optimal combination of the governing factors ($r = 4$ mm; $F_b = 200$ N; $f = 0.06$ mm/rev and $v = 200$ m/min), the obtained roughness is $R_a = 0.055$ μm . In other words, an SB of AISI 316Ti steel achieves a roughness, typical for the roller burnishing Ecoroll's process. Therefore, SB can be applied as a smoothing burnishing of chromium–nickel steels.

- SB of AISI 316Ti steel increases the superficial layer micro-hardness when the burnishing velocity v is smaller than 200 m/min. As velocity increases, micro-hardness decreases. Increasing the number of passes leads to an increase of the micro-hardness due to strain hardening of the material being slide burnished and the surface micro-hardness increase coefficient k_h is larger

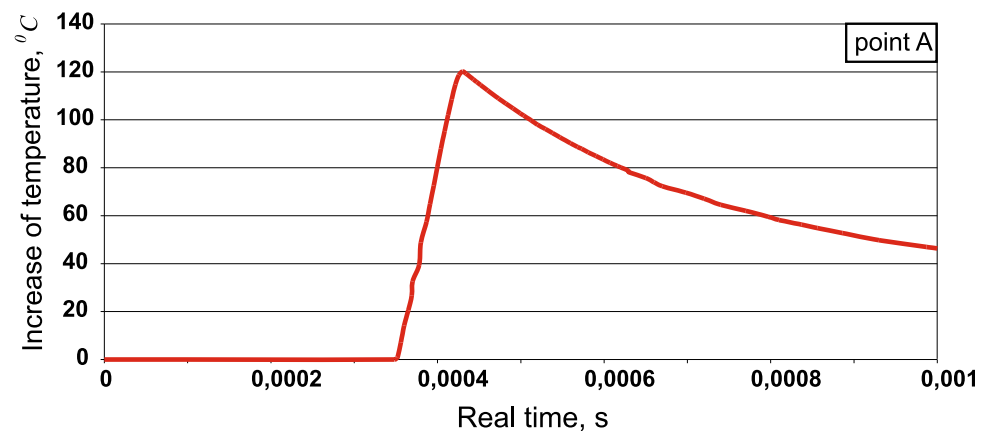
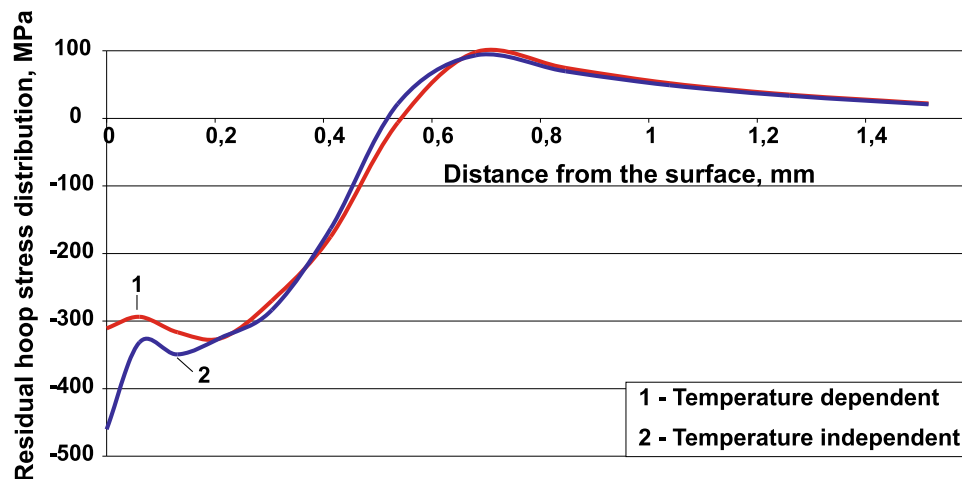
Fig. 16 Increase of the temperature in point A from the FE model

Fig. 17 Temperature-dependent residual hoop stress distribution



than 32%, whereby the resulting roughness is $R_a = 0.06 \mu\text{m}$. Hence, SB combines the achievement of very low roughness with significant cold work in a material's rim zone. As a result, the wear resistance of the slide burnished surface is significantly increased—the mass wear is more than 1.6 times less in comparison with a non-burnished surface.

- SB of AISI 316Ti steels introduces, in a significant depth, useful residual compressive stresses with a maximum absolute value that significantly exceeds the yield limit of the bulk material. This residual stress distribution is combined with very low roughness and significant cold work of the surface layer. This combination is typical for the deep rolling Ecoroll's process. Therefore, SB can be applied as mixed burnishing for finish treatment of chromium–nickel steels.
- SB leads to significant increase of 10^7 cycles fatigue strength (fatigue limit) of AISI 316Ti steel symmetrical rotational components, subjected cyclic bending fatigue tests. An increase of 38.9% has been achieved. At the same time fatigue life is increased more than 385 times.
- The greater burnishing velocity (more than 200 m/min) increases the productivity of processing, but on the other hand this velocity reduces the micro-hardness and residual stresses. Taking into account the known correlation [5] between micro-hardness and residual stresses on the one hand, and fatigue life on the other hand, it can be concluded that greater burnishing velocity reduces the fatigue life.

Acknowledgements This work was supported by the Bulgarian Ministry of Education and Science and the Technical University of Gabrovo under contract no 1702M. The authors would like to thank

Professor Mara Kandeveva from the Technical University in Sofia for her help with the wear tests. The authors would also like to acknowledge Dr. Yosiph Mitev for fatigue test specimens preparation.

References

1. Ecoroll Catalogue (2006) Tools and solutions for metal surface improvement. Ecoroll Corporation Tool Technology, USA
2. Korzynski M (2009) A model of smoothing slide ball-burnishing and an analysis of the parameter interaction. *J Mater Process Technol* 209(1):625–633
3. Korzynski M (2007) Modeling and experimental validation of the force-surface roughness relation for smoothing burnishing with a spherical tool. *Int J Mach Tools Manuf* 47(12):1956–1964
4. Maximov JT, Anchev AP, Duncheva GV, Ganev N, Selimov KF (2017) Influence of the process parameters on the surface roughness, micro-hardness and residual stresses in slide burnishing of high-strength aluminium alloys. *J Braz Soc Mech Sci Eng* 39(8):3067–3078
5. Maximov JT, Anchev AP, Dunchev VP, Ganev N, Duncheva GV, Selimov KF (2017) Effect of slide burnishing on fatigue performance of 2024-T3 high-strength aluminium alloy. *Fatigue Fail Eng Mater Struct* 40(11):1893–1904
6. Sai BW, Lebrun JL (2003) Influence of finishing by burnishing on surface characteristics. *J Mater Eng Perform* 12(1):37–40
7. Shiou FJ, Hsu CC (2008) Surface finishing of hardened and tempered stainless tool steel using sequential ball grinding, ball burnishing and ball polishing processes on a machining centre. *J Mater Process Technol* 205(1–3):249–258
8. Tian Y, Shin YS (2007) Laser assisted burnishing of metals. *Int J Mach Tools Manuf* 47(1):14–22
9. Shiou FJ, Huang SJ, Shih AJ, Zhu J, Yoshino Y (2017) Fine surface finish of a hardened stainless steel using a new burnishing tool. *Proc Manuf* 10:208–217
10. Labanowski J, Ossowska A (2006) Influence of burnishing on stress corrosion cracking susceptibility of duplex steel. *J Achiev Mater Manuf Eng* 19(1):46–52
11. Maximov JT, Anchev AP, Duncheva GV (2015) Modeling of the friction in tool-workpiece system in diamond burnishing process. *Coupled Syst Mech* 4(4):279–295